Article

Degradation of Alkali-Based Photocathodes from Exposure to Residual Gases: A First-Principles Study

Gaoxue Wang,[†,‡] Ravindra Pandey,[‡] Nathan A. Moody,[†] and Enrique R. Batista*,[†]

[†]Los Alamos National Laboratory, Los Alamos, New Mexico 87545, United States
[‡]Department of Physics, Michigan Technological University, Houghton, Michigan 49931, United States

Ⓢ *Supporting Information*

ABSTRACT: Photocathodes are a key component in the production of electron beams in systems such as X-ray free-electron lasers and X-ray energy-recovery linacs. Alkali-based materials display high quantum efficiency (QE), however, their QE undergoes degradation faster than metal photocathodes even in the high vacuum conditions where they operate. The high reactivity of alkali-based surfaces points to surface reactions with residual gases as one of the most important factors for the degradation of QE. To advance the understanding on the degradation of the QE, we investigated the surface reactivity of common residual gas molecules (e.g., O_2, CO_2, CO, H_2O, N_2, and H_2) on one of the best-known alkali-based photocathode materials, cesium antimonide (Cs_3Sb), using first-principles calculations based on density functional theory. The reaction sites, adsorption energy, and effect in the local electronic structure upon reaction of these molecules on (001), (110), and (111) surfaces of Cs_3Sb were computed and analyzed. The adsorption energy of these molecules on Cs_3Sb follows the trend of O_2 (−4.5 eV) > CO_2 (−1.9 eV) > H_2O (−1.0 eV) > CO (−0.8 eV) > N_2 (−0.3 eV) ≈ H_2 (−0.2 eV), which agrees with experimental data on the effect of these gases on the degradation of QE. The interaction strength is determined by the charge transfer from the surfaces to the molecules. The adsorption and dissociation of O containing molecules modify the surface chemistry such as the composition, structure, charge distribution, surface dipole, and work function of Cs_3Sb, resulting in the degradation of QE with exposure to O_2, CO_2, H_2O, and CO.
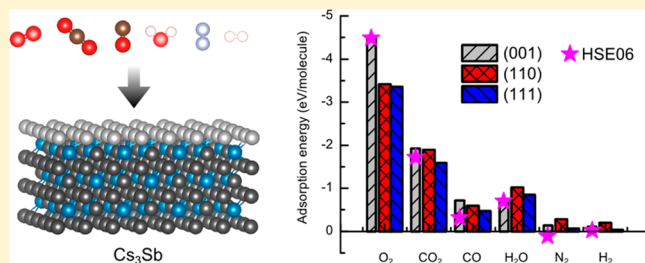
1.0. INTRODUCTION

Alkali-based photocathodes with high quantum efficiency (QE) in the visible spectrum are promising candidates for high quality electron beams for X-ray free-electron laser (XFEL) and energy-recovery linacs (XERL).[1] However, they are also known to suffer from fast degradation of QE under ultrahigh vacuum (UHV) conditions, even in the absence of illumination.[2−6] In general, surface reaction with residual gases in the vacuum chamber is one of the most important factors in determining the stability and shelf life of photocathodes containing alkali metals.[7] Therefore, a clear understanding of the interaction of gas molecules with photocathodes is necessary to suppress or eliminate the degradation of the QE.

Previously, the contaminating effect due to residual gases was investigated by exposing the photocathodes to individual gas species under controlled conditions.[5,8−12] As early as 1969, Decker studied the decay characteristics of alkali-Sb photocathodes exposed to residual environment gases.[13] Later, the poisoning effect on Cs_3Sb photocathodes was investigated by a few other groups.[2,12] The discovery of negative electron affinity (NEA) GaAs-Cs photocathode has stimulated more interest in the degradation of alkali-based photocathodes in the community.[5,8,9,11,14] It has been demonstrated that oxygen containing molecules, such as O_2, CO_2, CO, and H_2O, produce significant degradation to the QE, while N_2 and H_2 have no

effect to the QE.[2,5,8,9,11,14,15] Based on these experiments, it has been proposed that O_2, CO_2, and H_2O experience dissociative adsorption on the surface of alkali-based photocathodes, while CO adsorbs molecularly on the surface without dissociating into C and O atoms.[5,8] The O atoms dissociated from the O_2, CO_2, and H_2O molecules change the surface chemistry by deviating from the optimum Cs/O composition ratio and results in strong reduction of the QE.[5,8,10] Recently, a theoretical kinetic model was presented that describes the experimental data of QE degradation on the basis of three thermodynamic states: a desorbed gas molecule, a physisorbed state, and a reacted chemisorbed state.[6] Whereas these experiments provide data on the kinetics of gases interacting with photocathodes, which is confirmed with the kinetic model mentioned above,[6] no comprehensively theoretical efforts have been undertaken to elucidate the underlying physics and chemistry involved in the degradation process.

The present study seeks to advance the understanding of the degradation mechanism of alkali-based photocathodes upon exposure to residual gases. The interaction of common residual gases (O_2, CO_2, CO, H_2O, N_2, and H_2) with one well-known

alkali-based photoemitter, Cs_3Sb, was explored using first-principles calculations based on density functional theory. The reaction sites, adsorption energy, and effect in the local electronic structure upon reaction of these molecules on (001), (110), and (111) surfaces of Cs_3Sb were computed and analyzed. To the best of our knowledge, this is the first theoretical investigation on the interaction of gas molecules with alkali-based photocathodes. Our results are important to interpret the experimental data and provide atomic-level insights into the degradation of photocathodes with exposure to residual gases. It should be pointed out that in the present study we focus on the adsorption of neutral gas molecules on pristine Cs_3Sb surfaces as a first step to understand the fundamental interaction of gases with alkali-based photocathodes. Other factors that are of importance in real accelerator applications, such as surface roughness, defects, heating of the cathodes, ion back bombardment, ionization of gases, and surface chemical activation, are not involved in our computational model.

2.0. COMPUTATIONAL MODELS AND METHODS

The calculations were performed with the use of density functional theory (DFT) and projector augmented-wave (PAW) method[16] as implemented in the Vienna ab initio simulation package (VASP).[17] Plane wave basis sets with a cutoff energy of 500 eV were employed.[16] The generalized gradient approximation (GGA) of Perdew−Burke−Ernzerhof (PBE)[18] functional was used to represent the exchange-correlation interaction. The van der Waals (vdW) dispersion based on DFT-D3 method of Grimme[19] was included in the calculations. The Sb $5s$ and $5p$; the Cs $5s$, $5p$, and $6s$ electrons were treated as valence electrons. The energy convergence was set to 10^{-6} eV, and the residual force on each atom was smaller than 0.01 eV/Å for structural relaxations.

Bulk Cs_3Sb crystallizes either in a hexagonal Na_3As structure or the cubic DO_3 structure.[20] In the present study, we focus on the cubic DO_3 structure, which has high photosensitivity.[20−22] As shown in Figure 1a, our calculations find the lattice constant
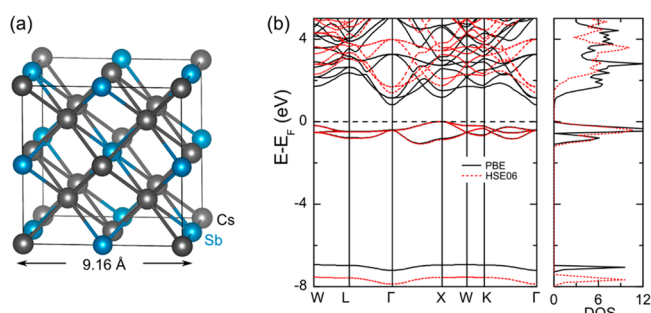
Figure 1. (a) Conventional cell and (b) electronic band structure of bulk Cs_3Sb with PBE or HSE06 functional.

of 9.16 Å, which is in excellent agreement with the experimental value of 9.128 Å (see Table 1).[23] The calculated electronic band structure of Cs_3Sb, as shown in Figure 1b, is consistent with previous reports that bulk Cs_3Sb is a semiconductor with an indirect band gap of 0.82 eV with the PBE functional.[21] It is already well-known that semiconductor band gaps are underestimated at GGA-DFT level of theory, hence, we further calculate the band structure of Cs_3Sb with the Heyd-Scuseria-Ernzerh (HSE06) hybrid functional, which incorporates the exact exchange.[24] The HSE06 hybrid functional improves the computed band gap to 1.39 eV, which is closer to the experimental value of 1.60 eV.[25] The bond lengths and formation energies of the considered gas molecules are listed in Table 2, which are also in excellent agreement with the experiments,[26] suggesting accuracy and reliability of the calculated results in the present study.

The surfaces of Cs_3Sb were represented in the three-dimensional periodic-boundary-condition simulation with a vacuum gap in the direction perpendicular to the surface. In the supercell, the vacuum distance normal to the slab was larger than 20 Å to eliminate the interactions between the replicas due to the periodic boundary conditions in the direction normal to the surface. The low index surfaces (001), (110), and (111) of Cs_3Sb were considered. The lateral dimensions of the simulations cells for the (001), (110), and (111) surfaces were 9.15×9.15, 9.15×12.95, and 12.95×12.95 (60°) Å^2, respectively. The reciprocal space was sampled by Monkhorst−Pack k points in the Brillouin zone with a grid of $(3 \times 3 \times 1)$, $(3 \times 2 \times 1)$, and $(2 \times 2 \times 1)$, respectively.

The adsorption energy of a gas molecule on the surfaces is defined as

$$E_{ads} = E_{total} - (E_{slab} + E_{molecule}) \tag{1}$$

where E_{slab} is the energy of the pristine slab, $E_{molecule}$ is the formation energy of the gas molecule, as listed in Table 2, and E_{total} is the total energy of the composite system after adsorption of gas molecules. By this definition, a negative value of E_{ads} corresponds to an exothermic process, which means the molecule will spontaneously adsorb on the surface.

In the initial configurations for the geometry optimization, the gas molecules were located over different surface sites 4 Å above the surface. Both parallel and vertical configurations of gas molecules on the surfaces were considered. During structural relaxation, the atoms in the top layers within a thickness of 5 Å were allowed to fully relax, and the rest of the atoms in the bottom layers were constrained. The dipole correction was included to nullify the artificial field imposed on the slab by the periodic boundary conditions.[29] No magnetic moment was found for the pristine surfaces or the composite systems after the adsorption of gas molecules in spin polarized calculations. Due to the high extra computational cost of using the hybrid functional HSE06,[24] we limited the use of this functional to single-point calculations at the PBE optimized geometries for band structure and for the molecular binding

Table 1. Comparison of the Calculated Lattice Constants and Formation Energies of Bulk Cs, Sb, and Cs_3Sb with Experimental Data

	bulk Cs		bulk Sb		bulk Cs_3Sb	
	lattice (Å)	energy (eV/atom)	lattice (Å)	energy (eV/atom)	lattice (Å)	energy (eV/Cs_3Sb)
PBE+DFT-D3	6.05	−0.94	4.33 10.98	−4.59	9.16	−8.94
experiment	6.141[27]		4.30 11.22[28]		9.128[23]	

Table 2. Comparison of the Calculated Bond Lengths and Formation Energies of Gas Molecules with Experimental Data[a]

	O_2	CO_2	CO	H_2O	N_2	H_2
formation energy (eV)	−9.87	−22.97	−14.78	−14.23	−16.64	−6.77
bond length (Å)	1.23	1.18	1.14	0.97	1.11	0.75
experimental bond length (Å)	1.21[26]	1.16[26]	1.13[26]	0.96[26]	1.10[26]	0.74[26]

[a]The calculated values are obtained at PBE+DFT-D3 level of theory.
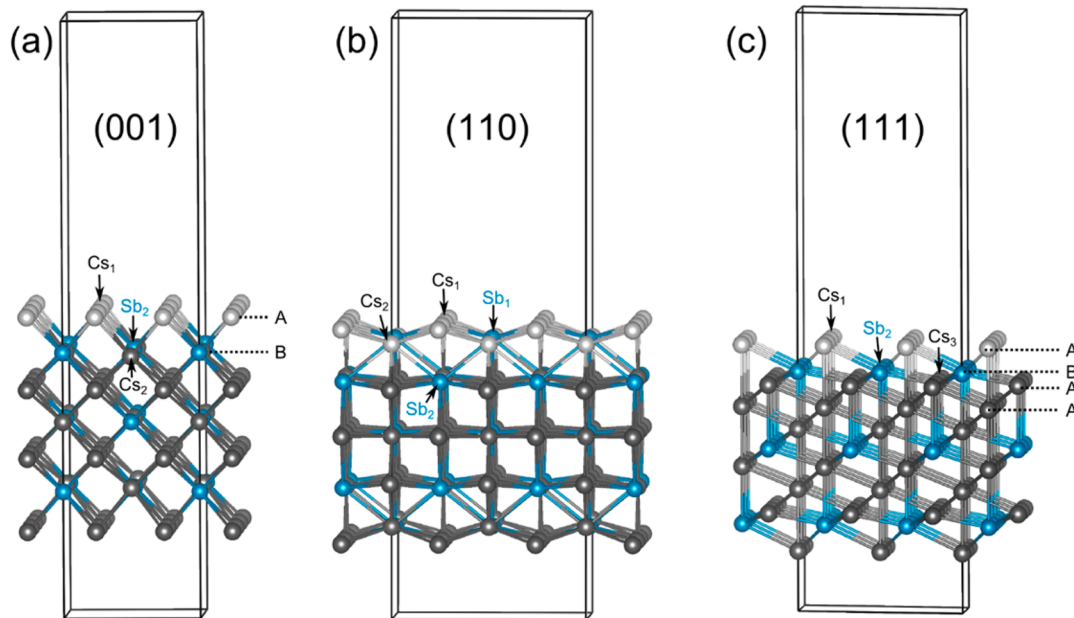
Figure 2. Slab models of the (001), (110), and (111) surfaces. The distinguished adsorption sites on each surface are illustrated with different labels. The thickness of the slabs is approximately 14.4 Å.

energy at the most stable configurations. Remarkably, the HSE06-computed energies are very close to the adsorption energies obtained from PBE, and they do not change the description instead yielding support to the PBE results.

3.0. RESULTS

3.1. Geometries and Surface Energies of Cs₃Sb. To study the relative stability of the different surfaces we employed a standard approach by comparing the surface energy defined as[30,31]

$$\gamma = \frac{1}{2A}(E_{slab} - n_{Cs} \times \mu_{Cs} - n_{Sb} \times \mu_{Sb}) \quad (2)$$

where E_{slab} is the total energy of the slab, n_{Cs}, and n_{Sb} are the number of Cs and Sb atoms in the slab, μ_{Cs} and μ_{Sb} are the chemical potential of Cs and Sb, respectively, A is the surface area, and γ can be considered as the energy for creating the surface, the most stable surface will minimize γ. Since the surfaces are in equilibrium with the underlying bulk material, the chemical potentials μ_{Cs} and μ_{Cs} are not independent, they are related via the expression: $3\mu_{Cs} + \mu_{Sb} = \mu_{Cs_3Sb}$. Here, μ_{Cs_3Sb} is the chemical potential of bulk Cs₃Sb per unit formula, which can be approximated by the total energy of bulk Cs₃Sb, E_{Cs_3Sb}. Substituting this into eq 2 yields the surface energy depending only on the chemical potential μ_{Cs}

$$\gamma = \frac{1}{2A}[E_{slab} - (n_{Cs} - 3n_{Sb}) \times \mu_{Cs} - n_{Sb} \times E_{Cs_3Sb}] \quad (3)$$

Considering the chemical potential μ_{Cs} and μ_{Sb} must be smaller than the energy of the atom in the corresponding stable bulk phase of Cs and Sb (as listed in Table 1)

$$\mu_{Cs} < E_{Cs}^{bulk}$$
$$\mu_{Sb} < E_{Sb}^{bulk} \quad (4)$$

we can obtain the upper and lower limits for the chemical potential μ_{Cs}

$$-1.45 \text{ eV} = \frac{E_{Cs_3Sb} - E_{Sb}^{bulk}}{3} < \mu_{Cs} < E_{Cs}^{bulk} = -0.94 \text{ eV} \quad (5)$$

The upper limit of μ_{Cs} corresponds to a Cs-rich condition, and the lower limit corresponds to a Cs-poor condition. The relative stability of the surfaces with different terminations is compared between the lower and upper limits of μ_{Cs}.

3.1.1. (001) Surface of Cs₃Sb. The (001) surface can have two kinds of terminations (see Figure 2a). One termination is comprised of only Cs atoms (labeled as "A"). The other termination is comprised of both Cs and Sb atoms (labeled as "B"). Three distinguished adsorption sites on this surface are labeled as Cs₁, Cs₂, and Sb₂, respectively.

The surface energy of A termination is plotted with solid black line in Figure 3, and the surface energy of B termination is plotted with dotted black line. It is found that the surface with A termination is more stable than the surface with B termination between the lower and upper limits of μ_{Cs}.
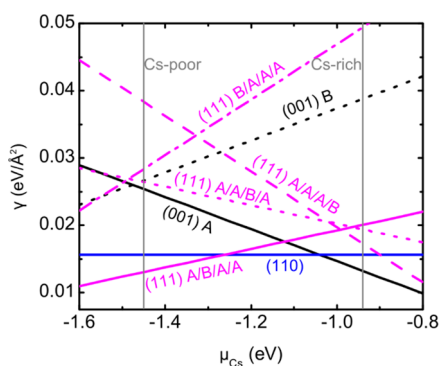
Figure 3. Surface energies of (001), (110), and (111) surfaces of Cs$_3$Sb with different terminations, the vertical lines represent the upper and lower limits for the chemical potential μ_{Cs}.

Therefore, (001) surface with A termination is considered for the subsequent calculations.

3.1.2. (110) Surface of Cs$_3$Sb. The (110) surface has only one kind of termination comprised of Cs and Sb with a composition ratio of 3:1. The surface energy of (110) face is constant as a function of μ_{Cs}, as shown with a solid blue line in Figure 3. The relaxed slab with (110) surfaces is shown in Figure 2b. Note that the outermost layer is reconstructed with the Cs atoms moving slightly outward the slab. Four distinguished sites labeled as Cs$_1$, Cs$_2$, Sb$_1$, and Sb$_2$ are considered for the adsorption of gas molecules on this surface.

3.1.3. (111) Surface of Cs$_3$Sb. Along the [111] direction, bulk Cs$_3$Sb is constituted by three layers of Cs (each of the Cs layer is labeled as "A") and one layer of Sb (labeled as "B") repeating in space. The (111) surface can be obtained by cleaving along any one of these layers. So, there are four kinds of possible terminations for this surface (e.g., A/A/A/B, A/A/B/A, A/B/A/A, and B/A/A/A). From the surface energy calculations, it is found that the surface with one Cs layer as the outermost layer, and the Sb layer as the second layer (the A/B/A/A termination) is preferred in most of the region between the lower and upper limits of μ_{Cs}, as illustrated with solid pink line in Figure 3. The surface energies for the other three terminations (A/A/A/B, A/A/B/A, and B/A/A/A) as illustrated with dashed pink lines are larger than that of the A/B/A/A termination. So, the (111) surface with A/B/A/A termination as shown in Figure 2c is considered for the adsorption of gas molecules. Three different adsorption sites Cs$_1$, Cs$_3$, and Sb$_2$ are considered for this surface.

From the surface energies in Figure 3, it is found that the (001) surface with A termination is the most stable surface in a Cs-rich condition. In the Cs-poor condition, close to the lower limit of μ_{Cs}, the (111) surface with A/B/A/A termination is more preferred. The (110) surface is more stable in the range from −1.25 to −1.04 eV for μ_{Cs}. Considering that the Cs$_3$Sb photocathode is fabricated by depositing Cs onto a film of Sb in experiments, it is likely that these facets will coexist in the samples due to the difficulty in controlling the stoichiometry at atomic level. Therefore, all these surfaces with the most stable terminations are considered to study the interaction with gas molecules.

3.2. O$_2$ Adsorption on (001) Surface of Cs$_3$Sb. Experimentally, O$_2$ has been shown to have the strongest or fastest degradation effect to the QE of alkali-based photocathodes among the investigated gas molecules.[5] This is explained as the direct reaction of O$_2$ with the photocathodes, which changes the surface chemistry and increases the energy barrier for electrons to escape from the surface to the vacuum.[5,32]

The computed equilibrium adsorption configurations of O$_2$ on (001) surface of Cs$_3$Sb are shown in Table 3. We identified

Table 3. Adsorption Configurations of O$_2$ on Different Sites of (001) Surface

	Cs$_2$		Sb$_2$		Cs$_1$	
	vertical	parallel	vertical	parallel	vertical	parallel
top view						
side view						
R_{O-O} (Å)	1.50	1.49	1.51	1.46	1.37	1.40
R_{Cs-O} (Å)	2.57	2.70	2.74	2.72	2.61	2.68
E_{ads} (eV)	-4.50	-4.09	-2.65	-2.31	-0.82	-1.38

three different adsorptions sites on this surface (see Figure 2a): Cs$_1$ corresponding to the site above a Cs atom on the top layer, Cs$_2$ on the exposed Cs of the second layer, and Sb$_2$ on the Sb atom of the second layer. The largest adsorption energy of −4.50 eV is found for the adsorption at the Cs$_2$ site in a vertical configuration. The large adsorption energy indicates strong chemical interactions between O$_2$ and Cs$_3$Sb. The adsorption at Cs$_2$ in the parallel configuration is slightly weaker than the vertical configuration with an adsorption energy of −4.09 eV. The adsorption energy at Sb$_2$ site is −2.65 eV for the vertical configuration, and −2.31 eV for the parallel configuration. The adsorption on top of Cs$_1$ has the lowest adsorption energy of −0.82 and −1.38 eV for the vertical and parallel configurations, respectively. In the most stable configuration, the O−O bond length is increased to 1.50 Å, which is a 24% increase compared to the O−O bond length in the free gas indicating oxidation of the surface and electron transfer from the Cs to the O$_2$ molecule. The shortest Cs−O bond length is found to be 2.57 Å.

To gain further insight into the interaction of O$_2$ with Cs$_3$Sb, we mapped the potential energy surface (PES) of O$_2$ molecule on the (001) surface as shown in Figure 4. The PES was obtained by fixing the lateral position of the O$_2$ molecule over the surface, and allowing the molecule to relax along the vertical direction. The surface atoms of the slab are fully optimized during this process. The energy minimum is found at the Cs$_2$ site, which implies this to be the energetically preferable adsorption site. The Sb$_2$ and Cs$_1$ sites are found actually to be local maxima, suggesting the adsorption of O$_2$ at Cs$_1$ and Sb$_2$ sites is not dynamically stable. Thus, O$_2$ molecules are expected to adsorb dominantly at Cs$_2$ sites. This is due to the high reactivity of alkali atoms at the surfaces, O$_2$ prefers to penetrate into the outermost Cs layer, so it can interact with neighboring Cs atoms as many as possible. A local minimum is also identified along the Sb$_2$−Cs$_1$ line with an adsorption energy of −3.5 eV. A molecule at this local minimum would have to overcome a barrier roughly 0.3 eV to migrate to the global minimum site Cs$_2$. From Bader charge analysis,[33] it is found that O$_2$ accepts 1.57 e$^-$ from the neighboring Cs atoms at the
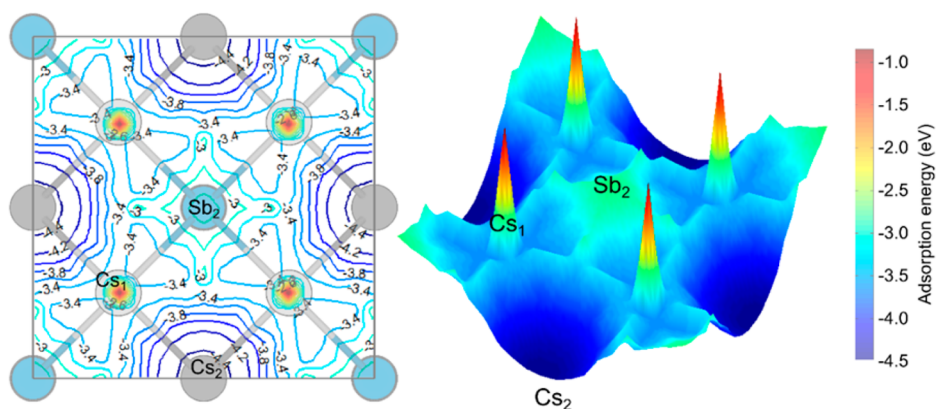
Figure 4. PES of O_2 molecule on (001) surface of Cs_3Sb. The left panel is the contour plot, the right panel is the 3D surface plot.

Cs_2 site. The charge transfer can be clearly seen in the charge redistribution plots in Figure S1 in the Supporting Information. The charge density increases around the O atoms and decreases in the region between Cs and O, indicating an ionic character of the bonds between Cs and O.

It has been proposed that an O_2 molecule may undergo dissociative adsorption on alkali-based photocathodes.[5,8] We calculated the dissociation energy of O_2 on the (001) surface of Cs_3Sb, as shown in Figure S2(a). The dissociation process of O_2 on this surface is found to be highly exothermic with a negative dissociation energy of −3.12 eV, which supports the dissociation of O_2, thus, the high reactivity of O_2 on alkali-based photocathodes.

Work Function. The work function plays a crucial role in determining the emittance of photocathodes.[34] It is the least energy required for an electron to escape from the surface to the vacuum, and can be expressed as $\Phi = E_{vacuum} - E_{Fermi}$, where E_{vacuum} is the vacuum level, and E_{Fermi} is the Fermi energy of the material. To check the effect of O_2 adsorption and dissociation on the QE of Cs_3Sb, the work function of the (001) surface with different level of O coverage were calculated. As shown in the inset of Figure 5a, the (2×2) model of the

Figure 5. (a) Work function and (b) surface dipole of (001) surface of Cs_3Sb with various coverage of O at the Cs_2 sites. A schematic model of the dipole is also shown in the insets of (b). The arrows indicate the direction of the surface dipole.

(001) surface contains eight Cs_2 sites, the coverage of O is defined as the ratio of the number of sites that are occupied by O atoms to the total number of Cs_2 sites. Due to the high reactivity of the Cs_2 sites, the coverage of O on these sites is expected to increase gradually with exposure to O_2.

The work function of the pristine (001) slab is calculated to be 2.1 eV, which agrees with the experimental value of 2.0 eV.[35] With a small amount of O coverage, the work function is found to decrease; and it gradually increases with O coverage larger

than 50% (Figure 5a). This indicates that a small amount of O adsorption on the (001) surface of Cs_3Sb should improve the QE of this surface, while the adsorption of more than 1/2 monolayer of O degrades the QE. The prediction from calculations is consistent with the experimental report that small amount of oxygen contaminant sensitizes the surface and causes an increase of the photocurrent of Cs_3Sb, whereas larger amounts of oxygen contaminant causes a decline of the photocurrent.[3]

The change of work function with different O coverage is strongly correlated to the surface dipole as shown in Figure 5b. In this figure, a positive value means the surface dipole is pointing out of the surface, while a negative value represents the dipole is pointing into the bulk. A small amount of O adsorption enhances the outward dipole, which contributes to the photoemission, while a large amount of O coverage weakens the outward dipole and even changes the direction of the dipole, thus, making photoemission more difficult. A schematic model of the surface dipole is shown in the insects of Figure 5b. The O atoms bind strongly to the surface with adsorption energy of −3.9 eV/O atom at a small oxygen coverage (see Figure S3(a) in the Supporting Information), and it decreases to −2.4 eV/O atom at a large oxygen coverage as a result of the competition among the adsorbed O atoms. The decrease in the adsorption energy is accompanied by the change in the relative positions of adsorbed O atoms and the top Cs atoms: the adsorbed O atoms are buried by neighboring Cs atom at a small amount of O coverage, while they tend to expose to the surface at a large amount of coverage as indicated by the relative position difference between the adsorbed O atoms and the Cs atoms in the top layer (see Figure S3(b) in the Supporting Information). The buried O atoms contribute to a dipole pointing outward the slab, and the exposed O atoms contribute to a dipole in the opposite direction. The result from the calculations are in line with the fact that Cs and O_2 could be used to activate NEA photocathodes, such as GaAs.[36,37] Cs and O could form an atomically Cs−O layer with low work function on the surface of GaAs, which benefits the electrons to escape to the vacuum thus increases the QE of photocathodes.[5,36,38] Work function of the Cs−O layer is sensitive to the composition ratio of Cs/O at the surface. Deviation from the optimum composition ratio will result in the increase of work function and deteriorate the performance of photocathodes.[36,37] The calculations reveal the significant roles of the surface chemical composition and the surface dipole to the work function, thus, the performance of photocathodes.

3.3. CO_2 Adsorption on (001) Surface of Cs_3Sb. CO_2 is another gas molecule that shows significant degradation effect to the QE of alkali-based photocathodes.[5,9] It has been proposed that CO_2 experiences dissociative adsorption on the surface,[14] however, direct evidence of the dissociation of CO_2 is still missing.

The adsorption configurations of CO_2 on (001) surface of Cs_3Sb are summarized in Table 4. The adsorption at Cs_2 site

Table 4. Adsorption Configurations of CO_2 on Different Sites of (001) Surface[a]

	Cs_2		Sb_2		Cs_1	
	vertical	parallel	vertical	parallel	vertical	parallel
top view						
side view						
R_{C-O} (Å)	1.29	1.30	1.18	1.26	1.18	1.18
R_{Cs-O} (Å)	2.77	2.73	3.85	2.96	3.27	3.98
R_{Cs-C} (Å)	3.02	3.03	4.62	3.82	4.45	3.81
$\angle_{O-C-O}$ (°)	121.2	119.2	180.0	129.8	180.0	178.9
E_{ads} (eV)	-1.81	-1.92	-0.21	-0.49	-0.14	-0.17

[a]Note that the "parallel" or "vertical" means the initial configuration of CO_2 on the surfaces before structural relaxation.

has the largest adsorption energy of −1.81 and −1.92 eV for the vertical and parallel configurations, respectively. The adsorption energy at the Sb_2 site is −0.21 and −0.49 eV for vertical and parallel configurations. At the Cs_1 site, the lowest energy is found to be −0.14 and −0.17 eV. For the adsorption at Cs_2 site, the CO_2 molecule is found to be bent, and the C−O bond length is increased to 1.30 Å as compared to 1.18 Å in the free gas. From Bader charge analysis,[33] it is found that CO_2 attracts 1.53 e⁻ from the surface, and most of the transferred electrons are concentrated on the C atom. The charge transfer can also be clearly seen in the charge redistribution plots in Figure S1 in the Supporting Information. The large adsorption energy and significant charge transfer indicate strong chemical interactions between CO_2 and the (001) surface of Cs_3Sb. The shortest bond for Cs−O and Cs−C is 2.73 and 3.02 Å, respectively. The dissociation of CO_2 into CO and O species on this surface is found to be endothermic with an energy gain of 0.48 eV (see Figure S2(b) in the Supporting Information), suggesting that CO_2 does not readily dissociate on these surfaces.

3.4. CO Adsorption on (001) Surface of Cs_3Sb. The effect of CO on the QE of alkali-based photocathodes is still under debate in the literature. Wada et al.[9] have shown that CO has no effect on the QE of NEA photocathode GaAs. While minor and slow degradation effects on the QE were observed by Chanlek et al.[5,11] in a more sophisticated vacuum system with a lower base pressure.

The adsorption configurations of CO on (001) surface of Cs_3Sb are shown in Table 5. Note that the vertical and parallel adsorption of CO at the Cs_2 site is relaxed to the similar final configuration with adsorption energy of −0.71 eV. The adsorption at Sb_2 site has lower adsorption energy of −0.29

Table 5. Adsorption Configurations of CO on Different Sites of (001) Surface

	Cs_2		Sb_2		Cs_1	
	vertical	parallel	vertical	parallel	vertical	parallel
top view						
side view						
R_{C-O} (Å)	1.21	1.21	1.16	1.18	1.16	1.21
R_{Cs-O} (Å)	3.74	3.57	4.70	3.27	4.46	3.60
R_{Cs-C} (Å)	3.13	3.13	3.92	3.33	3.30	3.14
E_{ads} (eV)	-0.71	-0.71	-0.29	-0.39	-0.24	-0.70

and −0.39 eV for the vertical and parallel configuration, respectively. At the Cs_1 site, the adsorption energy is −0.24 eV for the vertical configuration, and the adsorption with parallel configuration is relaxed to the similar structure to the adsorption at Cs_2 site. We have also considered the vertical adsorption configurations of CO with the O atom closer to the surface, which are found to have much smaller adsorption energies than the corresponding configurations with C atom closer to the surface. The C−O bond in the most stable configuration is elongated to 1.21 Å as compared to 1.13 Å in the free gas. The shortest distance from Cs to O and C are fairly large, 3.27 and 3.13 Å, respectively, which are longer than the corresponding distances for the adsorption of O_2 and CO_2. Bader charge analysis[33] indicates a 0.75 e⁻ transferred from the surface to the molecule. The adsorption energy of CO is much smaller than that of O_2 or CO_2 implying a considerably weaker interaction between CO and Cs_3Sb, which will lead to a faster desorption kinetics of CO under vacuum conditions. Moreover, the dissociation of CO to C and O atoms on this surface is found to be endothermic with a large energy gain of 1.53 eV (see Figure S2(c) in the Supporting Information), implying CO could not dissociate on alkali-based photocathodes at room temperature. Therefore, the CO molecule shows relatively slower degradation effect to the QE of alkali-based photocathodes than O_2 and CO_2.

3.5. H_2O Adsorption on (001) Surface of Cs_3Sb. Durek et al.[14] have studied the effect of water vapor on the photoemission of NEA photocathodes by introducing water vapor into the UHV system. They found that water vapor has a strong poisoning effect to photocathodes, and the lifetime of photocathodes is inversely proportional to the partial pressure of water vapor.[14]

The computed adsorption configurations of H_2O on the (001) surface of Cs_3Sb are summarized in Table 6. For H_2O adsorption, only the parallel adsorption in the initial configurations is considered. The largest adsorption energy is found to be −0.78 eV at the Sb_2 site. The H_2O lone pairs point toward one Cs atom on the top layer, and one H atom points toward the Sb in the second layer. The adsorption at Cs_2 and Cs_1 sites has lower adsorption energy of −0.58 and −0.34 eV, respectively. The H−O bond is elongated to 1.00 Å as compared to 0.97 Å in the gas phase, and the bond angle of the H_2O molecule is slightly changed. From Bader charge analysis[33]

Table 6. Adsorption Configurations of H₂O on Different Sites of the (001) Surface

	Cs₂	Sb₂	Cs₁
top view			
side view			
R_{C-O} (Å)	0.99	1.00	0.98
R_{Cs-O} (Å)	3.15	3.08	3.01
$\angle_{O-C-O}$ (°)	104.1	106.9	105.9
E_{ads} (eV)	-0.58	-0.78	-0.34

there is 0.26 e⁻ transfer from the surface to the molecule. The adsorption energy of H₂O on this surface is, however, rather weak, slightly larger than that of CO, and considerably smaller than the values for O₂ and CO₂. The lower adsorption energy is also reflected by the larger distance of 3.01 Å between Cs and O as compared to 2.57 Å for the Cs—O bonds in O₂ adsorption. The dissociation of H₂O on Cs₃Sb into OH + H was found to be highly exothermic with an energy release of −2.04 eV (see Figure S2(d) in the Supporting Information). Although the adsorption energy of H₂O molecule is only slightly larger than that of CO, it has been shown to have more serious degradation effect to the QE than CO. We hypothesize that this degradation is the result of chemisorption of the water dissociation products on the surface of Cs₃Sb, which contributes to the high reactivity of H₂O on alkali-based photocathodes. Further verification of this hypothesis requires the calculation of reaction activation energies and rates, which is outside the scope of this paper.

3.6. N₂ and H₂ Adsorption on the (001) Surface of Cs₃Sb. N₂ and H₂ molecules do not show obvious degradation effect to the QE of alkali-based photocathodes.[5] The adsorption configurations of N₂ and H₂ on (001) surface of Cs₃Sb are shown in Tables 7 and 8. Our calculations also find the adsorption energy of N₂ and H₂ is less than −0.14 eV for N₂

Table 7. Adsorption Configurations of N₂ on Different Sites of the (001) Surface

	Cs₂		Sb₂		Cs₁	
	vertical	parallel	vertical	parallel	vertical	parallel
top view						
side view						
R_{N-N} (Å)	1.12	1.12	1.13	1.14	1.12	1.13
R_{Cs-N} (Å)	5.15	4.92	3.98	3.52	3.39	3.60
E_{ads} (eV)	-0.01	-0.03	-0.13	-0.14	-0.10	-0.08

Table 8. Adsorption Configurations of H₂ on Different Sites of the (001) Surface

	Cs₂		Sb₂		Cs₁	
	vertical	parallel	vertical	parallel	vertical	parallel
top view						
side view						
R_{C-O} (Å)	1.29	0.75	0.78	0.75	0.75	0.75
R_{Cs-H} (Å)	5.21	4.23	3.26	3.91	4.12	3.68
E_{ads} (eV)	-0.02	-0.01	-0.11	-0.02	-0.01	-0.02

and less than −0.11 eV for H₂. The distance from Cs to N and H is longer than 3.39 and 3.26 Å, respectively. The small adsorption energy and large distances suggest the vdW force is dominating the interaction between N₂ and H₂ molecules and Cs₃Sb. Such vdW interaction has limited effects on the surface chemistry of photocathodes. Thus, alkali-based photocathodes are found to be inert to N₂ and H₂.

4.0. DISCUSSIONS

The adsorption energies of O₂, CO₂, CO, H₂O, N₂, and H₂ on (001), (110), and (111) surfaces of Cs₃Sb are summarized in Figure 6. The equilibrium adsorption configurations of gas
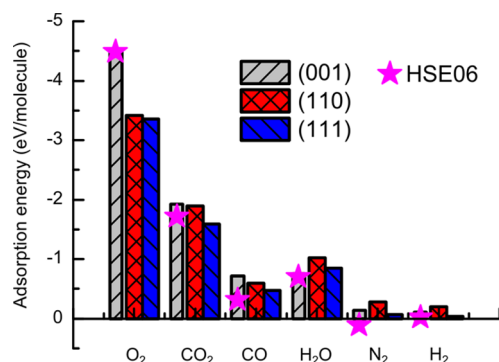
Figure 6. Adsorption energies of gas molecules on different surfaces of Cs₃Sb. The results with the HSE06 hybrid functional are illustrated with a star.

molecules on (110) and (111) surfaces can be found in Tables S1−S12 in the Supporting Information. Overall, the largest adsorption energies on these surfaces follow the trend of O₂ (−4.5 eV) > CO₂ (−1.9 eV) > H₂O (−1.0 eV) > CO (−0.8 eV) > N₂ (−0.3 eV) ≈ H₂ (−0.2 eV), which is in agreement with the experimental data.[5] The adsorption energy values computed with the more accurate HSE06 hybrid functional for O₂, CO₂, H₂O, CO, N₂, and H₂ on the (001) surface are −4.49, −1.71, −0.69, −0.31, 0.11, and −0.01 eV, respectively. These values are only slightly smaller than the results from PBE functional (Figure 6). The interaction strength is closely related to the charge transfer between Cs atoms and the molecules as shown in Figures 7 and S1 in the Supporting Information. The highly reactive Cs atoms at the surface of photocathodes could
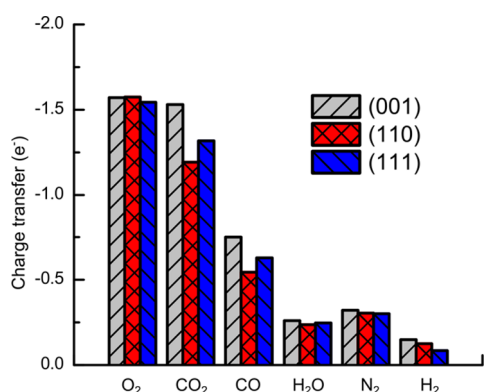
Figure 7. Charge transfer from (001), (110) and (111) surface of Cs$_3$Sb to O$_2$, CO$_2$, CO, H$_2$O, N$_2$, and H$_2$.

easily lose their valence electrons, the interaction strength of gas molecules with alkali-based photocathodes tends to be stronger for molecules that can accept extra electrons.

It is well-known that the O$_2$ molecule has a positive electron affinity of 0.45 eV,[39] thus, it prefers to accept electrons from photocathodes and binds strongly with the surface Cs atoms. The transferred electrons will occupy the antibonding orbital of O$_2$ molecule leading to the weakening and ultimately dissociation of the molecule. For CO$_2$, although it has a negative electron affinity of −0.6 eV,[40] it has been shown that materials with low work function, such as alkali atoms covered materials, are reactive with CO$_2$.[41,42] Our calculations find an average of ~1.3 e$^−$ transfer from the surface of Cs$_3$Sb to the CO$_2$ molecule. The transferred electrons occupy the lowest unoccupied orbital and result in the bending of the molecule in most of the adsorption configurations.[43] Therefore, CO$_2$ also has high reactivity toward alkali-based photocathodes with adsorption energy of −1.9 eV.

O$_2$ and CO$_2$ could significantly change the surface structure of alkali-based photocathodes due to their strong interaction with the surfaces. For example, O$_2$ and CO$_2$ could attract the neighboring Cs atoms forming cluster like structures at most sites on (110) surface as seen in Tables S1 and S2 in the Supporting Information. Considering the microcrystalline/amorphous structure of the photocathodes fabricated in experiments, the adsorbed O$_2$ and CO$_2$ molecules will most likely attract the nearby alkali atoms, resulting in the formation of complex structures on the surfaces altering their electronic properties. The surface chemistry of photocathodes is expected to significantly change due to the variation in the composition and structure after the adsorption of these molecules. Therefore, the QE of the alkali-based photocathodes is sensitive to the exposure of O$_2$ and CO$_2$.

For CO molecule, the adsorption energy on Cs$_3$Sb is around −0.8 eV, and ~0.6 e$^−$ is transferred from the surfaces to the molecule. The adsorption energy and charge transfer of CO are smaller than that of O$_2$ and CO$_2$, which enables the desorption of CO from the surfaces. In the meantime, the large positive dissociation energy of 1.53 eV indicates that CO molecule prefers to adsorbed molecularly on the surfaces of Cs$_3$Sb, resulting in slower degradation effects to the QE. For H$_2$O molecule, its adsorption energy is approximately −1.0 eV, which is slightly larger than that of CO. However, H$_2$O is expected to dissociate on Cs$_3$Sb into the more reactive OH and H fragments, with an energy release of −2.04 eV, which we

think is the source of the QE degradation induced by residual H$_2$O.

For N$_2$ and H$_2$, the adsorption energy on Cs$_3$Sb is smaller than −0.3 eV, and the charge transfer is less than ~0.4 e$^−$. Thus, N$_2$ and H$_2$ are interacting with the alkali-based photocathodes physically and do not show obvious degradation effect to the QE.

5.0. CONCLUSIONS

For the first time, first-principles calculations based on DFT are performed to understand the degradation of the QE of alkali-based photocathodes with exposure to residual gases. The adsorption energy of gas molecules on alkali-based photocathodes follows the trend O$_2$ > CO$_2$ > H$_2$O > CO > N$_2$ ≈ H$_2$, which agrees well with the experimental data. The interaction strength is found to be related to the charge transfer from the surface alkali atoms to the molecules. O$_2$ and CO$_2$ could bind strongly on alkali-based photocathodes, resulting in significant change in the chemical composition and structure at the surfaces. Thus, the QE of alkali-based photocathodes are sensitive to O$_2$ and CO$_2$. The adsorption energy of CO is much smaller than that of O$_2$ and CO$_2$, which is in line with its slow degradation effect to the QE. H$_2$O has an adsorption energy slightly larger than that of CO, while it can dissociate on the surface accelerating the degradation of photocathodes. N$_2$ and H$_2$ interact physically with alkali-based photocathodes without obvious change to the QE. The work function of alkali-based photocathodes depends strongly on the composition ratio of Cs/O at the surface, which is ascribed to the change of surface dipole with O adsorption. The results from present study demonstrate first-principles method to be a powerful tool for interpreting the experimental results on photocathodes. These theoretical calculations can be utilized to predict the performance of new photocathodes, ultimately leading to the design of high performance photocathodes in the future.

■ ASSOCIATED CONTENT

Ⓢ Supporting Information

The Supporting Information is available free of charge on the ACS Publications website at DOI: 10.1021/acs.jpcc.6b12796.

> Figure S1, Charge redistribution after adsorption of gas molecules on (001) surface of Cs$_3$Sb; Figure S2, Dissociation energy of gas molecules on (001) surface of Cs$_3$Sb; Figure S3, Adsorption energy and the relative position of O on the surface of Cs$_3$Sb; Tables S1−S6, Adsorption of gas molecules on (110) surface of Cs$_3$Sb; Tables S7−S12, Adsorption of gas molecules on (111) surface of Cs$_3$b (PDF).

■ AUTHOR INFORMATION

Corresponding Author

*E-mail: erb@lanl.gov.

ORCID Ⓞ

Enrique R. Batista: 0000-0002-3074-4022

Notes

The authors declare no competing financial interest.

■ ACKNOWLEDGMENTS

■ REFERENCES

(1) Carlsten, B. E.; et al. New Source Technologies and Their Impact on Future Light Sources. *Nucl. Instrum. Methods Phys. Res., Sect. A* **2010**, *622*, 657−668.

(2) Michelato, P. Photocathodes for Rf Photoinjectors. *Nucl. Instrum. Methods Phys. Res., Sect. A* **1997**, *393*, 455−459.

(3) Danielson, L. R.; Lee, C.; Oettinger, P. E. Laser Illuminated High Current Photocathodes. *Appl. Surf. Sci.* **1983**, *16*, 257−267.

(4) Pastuszka, S.; Terekhov, A. S.; Wolf, A. 'Stable to Unstable' Transition in the (Cs, O) Activation Layer on Gaas (100) Surfaces with Negative Electron Affinity in Extremely High Vacuum. *Appl. Surf. Sci.* **1996**, *99*, 361−365.

(5) Chanlek, N.; Herbert, J.; Jones, R.; Jones, L.; Middleman, K.; Militsyn, B. The Degradation of Quantum Efficiency in Negative Electron Affinity Gaas Photocathodes under Gas Exposure. *J. Phys. D: Appl. Phys.* **2014**, *47*, 055110.

(6) Pavlenko, V.; Liu, F.; Hoffbauer, M. A.; Moody, N. A.; Batista, E. R. Kinetics of Alkali-Based Photocathode Degradation. *AIP Adv.* **2016**, *6*, 115008.

(7) Sommer, A. Stability of Photocathodes. *Appl. Opt.* **1973**, *12*, 90−92.

(8) Sakai, J.; Mizutani, G.; Ushioda, S. Bonding of O_2, CO_2, and CO on a Cs/P-GaAs(100) Surface and Its Relation to Negative Electron Affinity. *Surf. Sci.* **1993**, *283*, 217−220.

(9) Tatsuaki, W.; Toshiyuki, N.; Takashi, N.; Masahiro, M.; Minoru, H. Influence of Exposure to CO, CO_2 and H_2O on the Stability of Gaas Photocathodes. *Jpn. J. Appl. Phys.* **1990**, *29*, 2087.

(10) Su, C. Y.; Chye, P. W.; Pianetta, P.; Lindau, I.; Spicer, W. E. Proceedings of the International Conference on Solid Films and Surfaces Tokyo, Japan, 5−8 July 1978oxygen Adsorption on Cs Covered GaAs(110) Surfaces. *Surf. Sci.* **1979**, *86*, 894−899.

(11) Chanlek, N.; Herbert, J.; Jones, R.; Jones, L.; Middleman, K.; Militsyn, B. High Stability of Negative Electron Affinity Gallium Arsenide Photocathodes Activated with Cs and Nf3. *J. Phys. D: Appl. Phys.* **2015**, *48*, 375102.

(12) Springer, R. W.; Cameron, B. J. Photocathode Transfer and Storage Techniques Using Alkali Vapor Feedback Control. *Nucl. Instrum. Methods Phys. Res., Sect. A* **1992**, *318*, 396−400.

(13) Decker, R. Decay of S-20 Photocathode Sensitivity Due to Ambient Gases. Adv. Electron. *Adv. Electron. Electron Phys.* **1969**, *28*, 357.

(14) Durek, D.; Frommberger, F.; Reichelt, T.; Westermann, M. Degradation of a Gallium-Arsenide Photoemitting Nea Surface by Water Vapour. *Appl. Surf. Sci.* **1999**, *143*, 319−322.

(15) Bhide, G.; Rangarajan, L.; Bhat, B. Optimization of Some Parameters for High Efficiency Caesium-Antimony Semitransparent Photocathodes. *J. Phys. D: Appl. Phys.* **1971**, *4*, 568.

(16) Kresse, G.; Joubert, D. From Ultrasoft Pseudopotentials to the Projector Augmented-Wave Method. *Phys. Rev. B: Condens. Matter Mater. Phys.* **1999**, *59*, 1758−1775.

(17) Kresse, G.; Furthmüller, J. Efficiency of Ab-Initio Total Energy Calculations for Metals and Semiconductors Using a Plane-Wave Basis Set. *Comput. Mater. Sci.* **1996**, *6*, 15−50.

(18) Perdew, J. P.; Burke, K.; Ernzerhof, M. Generalized Gradient Approximation Made Simple. *Phys. Rev. Lett.* **1996**, *77*, 3865−3868.

(19) Grimme, S. Semiempirical Gga-Type Density Functional Constructed with a Long-Range Dispersion Correction. *J. Comput. Chem.* **2006**, *27*, 1787−1799.

(20) Wei, S.-H.; Zunger, A. Electronic Structure of M 3 I Sb-Type Filled Tetrahedral Semiconductors. *Phys. Rev. B: Condens. Matter Mater. Phys.* **1987**, *35*, 3952.

(21) Kalarasse, L.; Bennecer, B.; Kalarasse, F. Optical Properties of the Alkali Antimonide Semiconductors Cs_3Sb, Cs_2KSb, CsK_2Sb and K_3Sb. *J. Phys. Chem. Solids* **2010**, *71*, 314−322.

(22) Kalarasse, L.; Bennecer, B.; Kalarasse, F.; Djeroud, S. Pressure Effect on the Electronic and Optical Properties of the Alkali Antimonide Semiconductors Cs_3Sb, KCs_2Sb, CsK_2Sb and K_3Sb: Ab Initio Study. *J. Phys. Chem. Solids* **2010**, *71*, 1732−1741.

(23) Jack, K.; Wachtel, M. The Characterization and Crystal Structure of Caesium Antimonide, a Photo-Electric Surface Material. *Proceedings of the Royal Society of London A: Mathematical, Physical and Engineering Sciences*; The Royal Society, 1957; pp 46−60.

(24) Heyd, J.; Scuseria, G. E.; Ernzerhof, M. Hybrid Functionals Based on a Screened Coulomb Potential. *J. Chem. Phys.* **2003**, *118*, 8207−8215.

(25) Spicer, W. E. Photoemissive, Photoconductive, and Optical Absorption Studies of Alkali-Antimony Compounds. *Phys. Rev.* **1958**, *112*, 114−122.

(26) Weast, R. C.; Astle, M. J.; Beyer, W. H. *CRC Handbook of Chemistry and Physics*; CRC Press: Boca Raton, FL, 1988; Vol. 69.

(27) Weir, C.; Piermarini, G.; Block, S. On the Crystal Structures of Cs ii and Ga ii. *J. Chem. Phys.* **1971**, *54*, 2768−2770.

(28) Barrett, C.; Cucka, P.; Haefner, K. The Crystal Structure of Antimony at 4.2, 78 and 298 K. *Acta Crystallogr.* **1963**, *16*, 451−453.

(29) Bengtsson, L. Dipole Correction for Surface Supercell Calculations. *Phys. Rev. B: Condens. Matter Mater. Phys.* **1999**, *59*, 12301−12304.

(30) Singh-Miller, N. E.; Marzari, N. Surface Energies, Work Functions, and Surface Relaxations of Low-Index Metallic Surfaces from First Principles. *Phys. Rev. B: Condens. Matter Mater. Phys.* **2009**, *80*, 235407.

(31) Reuter, K.; Scheffler, M. Composition, Structure, and Stability of $RuO_2(110)$ as a Function of Oxygen Pressure. *Phys. Rev. B: Condens. Matter Mater. Phys.* **2001**, *65*, 035406.

(32) Zou, J.; Chang, B.; Yang, Z.; Qiao, J.; Zeng, Y. Stability and Photoemission Characteristics for GaAs Photocathodes in a Demountable Vacuum System. *Appl. Phys. Lett.* **2008**, *92*, 172102.

(33) Henkelman, G.; Arnaldsson, A.; Jónsson, H. A Fast and Robust Algorithm for Bader Decomposition of Charge Density. *Comput. Mater. Sci.* **2006**, *36*, 354−360.

(34) Budde, M.; Gillespie, A.; Jarque, E. C.; Lecesne, N.; Welsch, C. P.; Xiang, R.; Teichert, J. International Conference on Laser Applications at Accelerators, La3net 2015, 25−27 March 2015, Mallorca, Spainphotocathodes for High Brightness Photo Injectors. *Physics Procedia* **2015**, *77*, 58−65.

(35) Teichert, J.; Xiang, R.; Suberlucq, G.; Verschuur, J. W. Report on Photocathodes. CARE Note–2004−033-PHIN, https://www.hzdr.de/projects/CARE/index.files/reports/report.pdf.

(36) Fisher, D. G.; Enstrom, R. E.; Escher, J. S.; Williams, B. F. Photoelectron Surface Escape Probability of (Ga,in)As: Cs−O in the 0.9 to [Inverted Lazy S] 1.6 Mm Range. *J. Appl. Phys.* **1972**, *43*, 3815−3823.

(37) Vergara, G.; Gómez, L. J.; Capmany, J.; Montojo, M. T. Adsorption Kinetics of Cesium and Oxygen on GaAs(100). *Surf. Sci.* **1992**, *278*, 131−145.

(38) Calabrese, R.; et al. Surface Analysis of a Gaas Electron Source Using Rutherford Backscattering Spectroscopy. *Appl. Phys. Lett.* **1994**, *65*, 301−302.

(39) Travers, M. J.; Cowles, D. C.; Ellison, G. B. Reinvestigation of the Electron Affinities of O_2 and NO. *Chem. Phys. Lett.* **1989**, *164*, 449−455.

(40) Compton, R.; Reinhardt, P.; Cooper, C. Collisional Ionization of Na, K, and Cs by CO_2, COS, and Cs_2: Molecular Electron Affinities. *J. Chem. Phys.* **1975**, *63*, 3821−3827.

(41) Burghaus, U. Surface Chemistry of CO_2−Adsorption of Carbon Dioxide on Clean Surfaces at Ultrahigh Vacuum. *Prog. Surf. Sci.* **2014**, *89*, 161−217.

(42) Hadenfeldt, S.; Benndorf, C.; Stricker, A.; Töwe, M. Proceedings of the 15th European Conference on Surface Scienceadsorption of CO_2 on K-Promoted Cu(111) Surfaces. *Surf. Sci.* **1996**, *352*, 295−299.

(43) Freund, H.-J.; Roberts, M. W. Surface Chemistry of Carbon Dioxide. *Surf. Sci. Rep.* **1996**, *25*, 225−273.